A CYCLIC P-Y PLASTICITY MODEL APPLIED TO PILE FOUNDATIONS IN SAND

By, Jung In Choi[1], Myoung Mo Kim[2], and Scott J. Brandenberg[3], M. ASCE

ABSTRACT

The lateral response of pile foundations in sand is commonly analyzed using the beam on nonlinear Winkler foundation assumption, with load transfer behavior often characterized by the API sand p-y relationship. The API relationship was developed for static loading conditions, with cyclic correction factors intended to represent degradation due to many slow loading cycles. However, the API model is often applied for dynamic loading conditions (e.g., earthquake shaking) because suitable alternatives have not been formulated. This study demonstrates that the API sand functional form is not ideal for dynamic analysis of piles, and presents a new functional form that better captures the nonlinear p-y behavior of piles in sand during earthquake loading. The new functional form is developed using bounding surface plasticity theory and implemented in OpenSees, an open source finite element modeling platform that is freely available to users. The proposed p-y model is shown to capture the experimental response of a pile from a centrifuge test program using calibrated model parameters.

Keywords: BNWF analysis, p-y curve, bounding surface plasticity, centrifuge models, dynamic analysis

[1] Senior Engineer, Central Research Institute, Samsung Heavy Industries Co., LTD., 80 Jangpyeong 3ro, Geoje Si, Gyeonsangnam Do, 656-710, Korea, E-mail: next2u00@snu.ac.kr
[2] Professor, Department of Civil Engineering, Seoul National University, San 56-1, Shinlim-Dong, Kwanak-Ku, Seoul, 151-742, Korea. E-mail: geotech@snu.ac.kr
[3] Associate Professor and Vice Chair, Department of Civil and Environmental Engineering, University of California, Los Angeles, 5731 Boelter Hall, Los Angeles, CA 90095-1593 (corresponding author). E-Mail: sjbrandenberg@ucla.edu

INTRODUCTION

The beam on a nonlinear Winkler foundation (BNWF) analysis method is the most common approach to analyzing the behavior of laterally loaded pile foundations. The BNWF procedure models horizontal interaction between piles and soil using macro-elements (herein called p-y elements) that are assumed to act independently of the adjacent elements above and below. Although the assumption of macro-element independence does not rigorously capture the continuum behavior, the BNWF solution is still widely utilized because it is much simpler than continuum modeling. The properties of the p-y elements depend on soil strength and stiffness, pile properties, kinematic loading conditions, and excitation frequency. Selection of appropriate p-y material properties is therefore very important for accurate BNWF modeling.

The p-y material models most commonly used in analysis of piles were formulated in the 1960's and 70's for static and slow cyclic loading conditions. Examples that are commonly used today include the API sand model (API 1993), and Matlock's models for clay (Matlock 1970). These models were based on the best available information at the time of their publication, but are not validated over a wide range of soil types, pile types, and loading conditions. Dynamic loading conditions encountered during earthquakes were not considered in the formulation of these p-y material models. The "cyclic" correction factors included in the material models were developed for many repeated slow-cyclic loading cycles rather than for dynamic loading conditions. However, these p-y models are often utilized for earthquake loading conditions because suitable alternatives have not been formulated.

Shortcomings of API sand model for dynamic problems

Recent research has identified several problems with application of the API sand model to dynamic problems, and we focus herein on three issues: ultimate capacity, initial stiffness, and the shape of the p-y relations.

Ultimate Capacity

A number of studies have demonstrated that the API sand equations tend to under-estimate ultimate capacity at shallow depths, and others have shown an over-prediction deeper in the profile. Under-predicting ultimate capacity may be conservative for problems in which an external load is imposed at the pile head, but may be either conservative or unconservative for dynamic problems. Underestimating p-y capacity, typically considered "conservative", may increase or decrease pile response depending on the system frequency response and ground motion characteristics. Therefore, accurately estimating ultimate capacity is important for dynamic problems.

Dobry et al. (2003) reported that the API p-y curve underestimates the ultimate resistance of a shallow crust layer resting atop liquefiable sand. Rollins et al. (2005) found that the API sand equations under-estimated mobilized loads, and suggested that peak friction angle should be computed using a differnet approach from the API suggestion. Their approach is to compute peak friction angle as a function of the anticipated mean effective stress at failure in accordance to critical state soil mechanics concepts explained by Bolton (1984). This approach resulted in higher friction angles at shallow depths and produced better agreement with measurments from their field test on a pile group in sand. Yang et al. (2011) and Yoo et al. (2013) found that the API p-y curve significantly underestimates the ultimate resistance of soil at shallow depths. McGann et al. (2011) performed three-dimensional finite element simulations of piles under deep kinematic loading conditions consistent with lateral spreading of a liquefied soil profile, and found that the API sand model significantly over-predicts p-y capacity deep in the profile, and slightly under-predicts capacity at shallow depths.

Initial Stiffness

In addition to the ultimate capacity of the API sand model, formulation of the stiffness is also problematic for dynamic problems. The subgrade reaction modulus, k, varies linearly in the API sand relation and is represented by a coefficient of modulus variation, η_h, that is a function of relative density. Note that $k = \eta_h \cdot x/B$, and values of η_h suggested in the API relation are based on the smallest measurable displacements from field tests, which are large enough to induce nonlinear response in the soil. The secant shear modulus for sand begins to degrade at very small strains as low as about 0.001% (e.g., Darendeli 2001). Kagawa and Kraft (1980) extended a relation by Matlock (1970) to define the maximum shear strain in the soil around a pile to the relative displacement as $\gamma_{ave} = (y/B)(1 + \nu)/2.5$. For a typical Poisson ratio for sand of $\nu = 0.35$, the onset of nonlinear behavior will therefore correspond to a normalized displacement of only $y_{yield}/B = 2\times10^{-5}$. For a 1-m diameter pile, displacements of 0.02mm would mobilize nonlinear behavior. This value is much smaller than the displacements that can be accurately measured in a field test, therefore, the η_h values represent a strain-compatible value. Errors in small strain stiffness may have little influence on many static loading problems where mobilized displacements are similar to those induced in field tests from which the relations were derived. However, errors in elastic stiffness may have significant influence on soil dynamics problems where mobilized displacements may be much smaller than those mobilized in static field tests. A more rational approach would therefore utilize measured shear wave velocity as an input to define the truly small-strain elastic subgrade reaction stiffness.

Furthermore, the API sand relation assumes that the subgrade reaction modulus varies linearly with depth, whereas the shear modulus of cohesionless sands is known to vary approximately with the square root of confining pressure (Hardin and Drnevich 1972, Yamada et al. 2008). Boulanger et al. (2003) and McGann et al. (2011) proposed corrections to the subgrade reaction modulus terms to capture the parabolic variation with confining pressure.

Shape of p-y Backbone Curve

In addition to the issues with the ultimate capacity and initial stiffness of the API sand p-y relations, recent research has demonstrated that the shape of the p-y relation may also be problematic. For example, Varun (2010) demonstrated that the API sand curve is too linear at small strain, and suggested an alternative form that resulted in better agreement with measurements. Brandenberg et al. (2013) showed that the API sand backbone relation could produce reasonable results if the initial stiffess was adjusted based on the intensity of shaking imposed on the base of a centrifuge model container. This intensity dependence indicates that the API functional form is not capturing the proper nonlinear backbone shape. Finally, Yang et al. (2011) and Yoo et al. (2013) found that the API sand relation overestimates the subgrade reaction modulus at shallow depths when the displacement of the pile is less than 1% of the pile diameter (but larger than the small-strain behavior).

PROPOSED UNIAXIAL P-Y CONSTITUTIVE MODEL

A uniaxial plasticity model of the nonlinear force-displacement response between laterally loaded piles and soil has been formulated following general principles of bounding surface plasticity (e.g., Dafalias 1986). This model overcomes some of the aforementioned shortcomings of the API sand model, as demonstrated later by comparison with measurements from a centrifuge test program. The two-surface model consists of a yield surface and a bounding surface, and defines the plastic modulus based on the distance in force-space between the current force and the force on the bounding surface along the current loading direction. A kinematic hardening law defines the evolution of the center of the elastic region, and the elastic region size remains constant (i.e., there is no isotropic hardening). The elasto-plastic modulus and algorithm modulus are identical since this is a one-dimensional plasticity model (e.g., Simo and Hughes 1998).

The components of the constitutive model include the elastic constitutive law (Eq. 1), the yield function (Eq. 2), the plastic modulus definition (Eq. 3), the kinematic hardening law (Eq. 4), and the elasto-plastic modulus (Eq. 5), where K^e is elastic modulus, K^p is plastic modulus, $\dot{\gamma}, \dot{\gamma}^e$, and $\dot{\gamma}^p$ are the displacement rate, elastic displacement rate, and plastic displacement rate, repsectively, p_α is the value of p at the center of the elastic region (analogous to the backstress is classical plasticity theory), p_y is the size of the yield surface, p_u is the size of the bounding surface, C is a material constant that depends on initial vertical effective stress, and p_{in} is the value of p at the start of the current plastic loading cycle. User inputs include K^e, p_y, p_u, and C, and guidance for selecting these input parameters is provided in the context of the centrifuge test pile presented in the next section.

Elastic constitutive law

$$\dot{p} = K^e \dot{y}^e = K^e \left(\dot{y} - \dot{y}^p \right) \tag{1}$$

Yield function

$$f = \left| p - p_\alpha \right| - p_y \tag{2}$$

Plastic modulus

$$K^p = C \cdot K^e \frac{\left| p_u \cdot sign(\dot{y}) - p \right|}{\left| p - p_{in} \right|} \tag{3}$$

Kinematic hardening law

$$\dot{p}_\alpha = K^p \dot{y}^p \tag{4}$$

Elasto-plastic modulus

$$K = \frac{\dot{p}}{\dot{y}} = \frac{K^p K^e}{K^p + K^e} \tag{5}$$

A schematic demonstrating evolution of the constitutive model is shown in Fig. 1, in which we assume that the initial state of the model is $p = p_\alpha = p_{in} = 0$ (Fig. 1a). Loading in the positive y-direction remains elastic until the force reaches the yield surface (Fig. 1b), at which point the value of p_{in} is updated to the value of p at the onset of yielding.

Note that the plastic modulus is infinite at the onset of yield because $|p\text{-}p_{in}|$ in the denominator of Eq. 3 is zero. This feature of behavior avoids the discontinuity in slope that would occur if the plastic modulus were finite at the onset of yield. As plastic loading continues (Fig. 1c) in the positive y-direction, the value of p_{in} does not change, and the yield surface evolves in accordance with the kinematic hardening law defined in Eq. 4. The tangent modulus decreases with increasing displacement because $|p\text{-}p_{in}|$ becomes finite and increases, and $\left|p_u \cdot sign(\dot{y}) - p\right|$ in the numerator of Eq. 3 decreases. When unloading occurs (Fig. 1d), the initial slope is equal to K^e and the behavior remains in the elastic region until the force reaches the lower yield surface (i.e., $p = p_\alpha - p_y$ from Fig. 1c) and then plastic unloading begins. The value of p_{in} is updated to be equal to the value of p at the start of the plastic loading cycle, and the curve becomes nonlinear. Note that the evolution of the plastic modulus now depends on the distance to the lower bounding surface since the direction of loading is negative.

The parameter, C, controls the shape of the p-y backbone curve, and can be either set to match experimental data, or set to match a desired value of y_{50} (i.e., the displacement where p = 0.5pu) using Eq. 6.

$$C = \frac{\left(p_u - p_y\right)\left[\ln\left(p_u - p_y\right) - \ln\left(p_u\right)\right] + p_u\left(\ln(2) - 0.5\right) + p_y\left(1 - \ln(2)\right)}{K^e y_{50} - 0.5 p_u} \tag{6}$$

The model is demonstrated in dimensionless form in Fig. 2 for a monotonic load path for a constant y_{50} and various values of K^e, and for a cyclic load path with $K^e = p_u/y_{50}$. Note that a value of $K^e = 0.5p_u/y_{50}$ is the minimum logically admissible value, which results in an elastic-perfectly plastic formulation that renders the modeling equation unstable (i.e., a condition of the model is that $K^e > 0.5p_u/y_{50}$). For all cases $p_y/p_u = 0.1$, and at the beginning of each loading sequence, $p = p_\alpha = p_{in} = 0$. For the monotonic load paths, each curve passes through the same y_{50} point and curves with higher K^e are more nonlinear and approach pu more slowly than curves with lower K^e. For the cyclic loading curve, some degradation is apparent in the hysteretic behavior due to the evolution of the p_{in} term. This is a well-known feature of this particular bounding surface plasticity modeling approach (e.g., Dafalias 1986).

The model is implemented in OpenSees (McKenna et al. 2010), an open source finite element modeling platform, and is called PySimple3. A closed-form return mapping algorithm is not achievable, so iteration is required to obtain the updated force condition for a given state of internal variables and displacement increment. An implicit integration scheme is adopted to solve the equations in a manner that makes the model numerically stable and insensitive to the size of the loading increment. For example, in Fig. 2 the solid line was obtained using 1000 increments (500 per cycle), whereas the circular symbols were obtained using only 16 time steps (8 per cycle). The points essentially lie on top of the line, which demonstrates the robustness of the implicit integration algorithm.

CENTRIFUGE EXPERIMENTS

Dynamic centrifuge model tests for a single pile were conducted at the Korea Construction Engineering Development Collaboratory Program (KOCED), Geo-Centrifuge Center, on a centrifuge which has a radius of 5 m, 2.5 ton payload and up to 100 g centrifugal acceleration (Kim et al. 2013a, Kim et al. 2013b). All tests in this study were carried out at a centrifugal acceleration of 40 g.

Fig. 3 shows the schematic layout of a single pile and instrumentation for the centrifuge tests. The model container used for the centrifuge tests was an Equivalent Shear Beam (ESB) box. The ESB model container was formed by stacking 10 light-weight aluminum alloy rectangular frames on a base plate to create internal dimensions of 49 cm × 49 cm × 63 cm and external dimensions of 65 cm × 65 cm × 65 cm in length, width, and height, respectively. Each frame is 6 cm in height and is separated by inside ball bearings and rubber spacing layers. The design concept is to replicate one-dimensional site response conditions, and the performance of the ESB box was presented by Lee et al. (2013). Although the container captures one-dimensional wave propagation conditions rather well, it imposes undesired boundary conditions with respect to waves propagating away from the piles. Rayleigh waves and p-waves emanating from the pile during vibration will reflect from the container walls. This may influence observed geometric (i.e., radiation) damping, and the "free-field" response may be altered as a result.

The model pile was fabricated with a closed-ended aluminum pipe with 2.5 cm external diameter and a 0.1 cm wall thickness. The pile was clamped to the base of the container forming essentially a pin connection. A 1.0 kg mass was attached to the pile with the centroid of the mass acting at the height of 14.25 cm above the ground surface. The properties of the soil-pile system are summarized in Table 1. Strain gauges were attached on both sides of the pile to measure curvature, from which bending moments were computed based on the observed elastic pile behavior. An accelerometer was attached to the superstructure mass.

The model soil was Jumoonjin sand, characterized as fine-grained uniform sand (Table 2). The dry sand deposit was prepared to have a relative density of D_r = 80% (γ = 15.8 kN/m^3) to minimize changes in relative density during the shaking sequence that could be significant for looser sand. A peak friction angle of 40° was measured in a triaxial compression device at confining pressures in the range from 100 to 300 kPa. The shear wave velocity of the sand was measured using bender elements, and was found to vary with vertical effective stress according to Eq. 7. The exponent on the confining pressure term is 0.282, which implies a dependence of shear modulus with the 0.564 power of confining pressure, which is reasonable for cohesionless sand.

$$V_S\,(m/\sec) = 214\left(\frac{\sigma_v'}{p_a}\right)^{0.282} \tag{7}$$

A sequence of sinusoidal excitations was imposed on the base of the model. The amplitude of the input motion varied from 0.05 g to 0.4 g and the frequency was 1.5 Hz in the prototype scale. Table 3 shows the test program.

EXPERIMENTAL P-Y CURVES

Lateral resistance p and pile displacement y_{pile} were calculated based on the Euler beam theory, as shown in equation (8)

$$p = \frac{d^2}{dz^2}M(z) \qquad\qquad y_{pile} = \iint \frac{M(z)}{EI}\,dz \tag{8}$$

where $M(z)$ is bending moment along a pile and EI is flexural stiffness. The weighted residual method (Brandenberg et al. 2010) was used to compute the lateral resistance p.

Pile displacement was determined by double integration of curvature along the pile using the trapezoidal rule, and the two required constants of integration were the measured pile head displacement (by double-integrating the recorded acceleration in time) and the measured pile tip displacement at the pin connection. The displacement *y* in the dynamic p-y curve is relative displacement between the soil and pile, therefore the horizontal soil displacement y_{soil} was computed by double-integrating the free field acceleration records in time. Values of y_{soil} were interpolated at the positons where y_{pile} were computed, and values of *y* were then obtained as y_{pile} - y_{soil}.

Several cycles of the experimental dynamic p-y curves at depths of 0.5 m and 1.5 m for various input acceleration amplitudes in prototype scale are shown in Fig. 4. The secant stiffness clearly decreases as shaking intensity increases. Furthermore, hysteretic damping (represented by the normalized area inside the p-y loop) increases as shaking intensity increases.

Backbone Curve

The back-calculated p-y data points for each shaking level form a backbone curve defined by the peaks in the p-y loops. The backbone curves are compared with the proposed model presented in this paper, and with the API sand model. The API sand curves were computed using the peak friction angle of 40° measured in triaxial compression tests, and the suggested value of η_h = 61,000 kN/m^3 corresponding to D_r = 80%.

For the material model presented in this paper, we select values of p_u to be consistent with the observations from the dynamic centrifuge test study by Yoo et al. (2013), who suggested that p_u can be computed using Eq. 9, where B is the pile diameter in cm, K_p is the passive pressure coefficient based on Rankine earth pressure theory, γ' is effective unit weight in N/cm^3, and z is depth in cm. This relation provides a reasonable fit at displacements within the range of interest for typical earthquake loading conditions.

$$p_u = 13.3 B K_P \gamma' z^{1.02} \tag{9}$$

Yoo et al. (2013) found that Eq. 9 reasonably matched the dynamic backbone curve obtained from dynamic shaking, but over-predicted the results of a static load test performed on the model pile (Fig. 5). The difference between static and dynamic capacities is not clear, but may be related to radiation damping or strain rate effects. More work is needed to better quantify this rate effect, and caution is suggested when interpreting centrifuge test data, where very high strain rates may be mobilized. Eq. 9 should not be used for static loading conditions as it is likely to significantly over-predict static capacity, and should not be used for dynamic problems until the rate effects are better understood.

Elastic stiffness is defined based on the shear wave velocity profile in Eq. 7 combined with the relation by Gazetas and Dobry (1984) defining subgrade reaction modulus in terms of the Young's modulus of the pile, E_p, and soil, E_s:

$$K^e = 1.69\left(\frac{E_p}{E_s}\right)^{-0.137} E_s \qquad (10)$$

The Young's modulus of the soil was computed as $E_s = 2\,\rho V_s^2\,(1+\nu)$, where we assumed ν=0.35. The value of E_p is based on the assumption that the pile cross section is constant and solid. The pile in this study was an aluminum tube, so E_p was selected as the value that matches the *EI* of the pile section assuming the cross-section is solid.

The yield displacement of the pile was computed by assuming that the shear strain at which the soil begins exhibiting plasticity is γ_{yield} = 0.001% (Darendeli 2001), and that $y_{yield} = 2.5B\gamma_{yield}/(1+\nu)$ following Kagawa and Kraft (1980). The yield force was then defined as $p_y = K^e y_{yield}$.

The harderning material constant, C, was adjusted to provide a good match for the centrifuge test data according to Eq. 11:

$$C = 0.015\left(\frac{\sigma_{vo}'}{p_a}\right)^{-0.564} \qquad (11)$$

This relation is calibrated to the particular pile and sand tested in the centrifuge modeling study, and more research is needed to provide values of C as a function of soil type, density, and possibly other factors that influence the shape of the p-y curve. In the meantime, users should exercise judgment in selecting C so that the resulting p-y curve is reasonable (e.g., by matching a published y_{50} value, or by adjusting C so that the p-y capacity is mobilized at a reasonable displacement).

A comparison of the experimental backbone curve with the PySimple3 material model, and with the API sand model is shown in Fig. 6 for depths of 0.5m and 1.5m. The API sand curve significantly under-estimates the ultimate capacity, and over-estimates the stiffness in the range below about y=0.01m. By contrast, the proposed model fits the data quite well.

BNWF ANALYSES

Experimental data are compared with beam on nonlinear Winkler foundation (BNWF) analyses performed in OpenSees using the new PySimple3 material and the PySimple1 material model with soilType = 2 formulated to match the API sand backbone curve. The pile is modeled utilizing 60 elastic beam-column elements evenly-distributed along the length of the pile, and p-y elements were distributed along the pile at 0.5m intervals beginning at a depth of 0.5m. The vertical displacement is fixed at the bottom of the pile, the horizontal displacement is set equal to the container base displacement, and the pile is free to rotate at its base. Input motions from recorded acceleration at various depths in the "free-field" soil (i.e., in the model container to the side of the pile, where pile influence is anticipated to be small) were imposed on the free-end of each p-y element. The analysis is conducted using the penalty method for constraints handler, the reverse Cuthill-McKee scheme for the numberer, the Newmark method for the integrator and convergence tolerance on the norm of the displacement residual was 10^{-9}. Full Rayleigh damping was used in the analysis, and 2% damping was used at the driving frequencies of the input ground motion, and at double that frequency in the analyses. Numerical damping was not applied within the Newmark integrator.

Fig. 7 shows measured and computed superstructure acceleration, and Fig. 8 compares snapshots of the bending moment profile at the time that the peak bending moment was measured for each input motion. The PySimple3 model produces reasonable agreement with the measured acceleration data, but slightly over-predicts the horizontal acceleration of the superstructure mass for input accelerations of 0.3 and 0.4g. By contrast, the API sand model causes much more erroneous predictions ranging from +76% for the 0.05g input motion to +47% for the 0.4g input motion. We observed that for each input intensity, we could select a specific stiffness for the API sand model that would provide a reasonable prediction. For example, η_h = 36700, 24500, and 13800 kN/m^3 produced reasonable agreement with the test data for input intensities of 0.05, 0.15, and 0.30g, respectively. However, this intensity dependence is an undesired effect. By contrast, the PySimple3 material model is able to reasonably capture the measured response for all of the shaking intensity levels using a single set of input parameters.

The PySimple3 material model begins to deviate from the measured response at about time = 10s during the 0.3g motion, with the computed amplitude becoming larger than measured. This trend then continues for the 0.4g input motion. We attribute this behavior to formation of a depression in the sand around the pile during large excitations. Gapping is known to influence p-y behavior in clay (e.g., Matlock et al.

1978), but granular soils are generally assumed to be non-susceptible to gapping effects due to their inability to maintain a vertical surface unsupported. However, formation of a depression around the pile can nevertheless influence the p-y response. Better agreement was achieved for the 0.3g and 0.4g input motions when the top p-y element (i.e., at a depth of 0.5m) was removed from the analysis (Fig. 9), which supports the conclusion that the depression explains the mismatch for the large motions. The apparent horizontal zone of influence for the depression formation is approximately 1m, which is also 1 pile diameter in this case.

The inset in Fig. 6 shows that the stiffness of the API sand relation is lower than the elastic stiffness of the PySimple3 material model. To ascertain the small-strain p-y stiffness in the centrifuge model, we turn to ambient vibrations recorded during the centrifuge test (strain gauge measurements do not provide adequate resolution in the small-strain region). Twenty separate windows of ambient vibration time were recorded, the transfer function between the horizontal motion of the superstructure and container base was computed for each case, and the averaged transfer function was smoothed in the frequency domain as shown in Fig. 10. The first-mode natural frequency of the pile was then computed for the numerical models as the first mode Eigenvalue.

The peak in the measured transfer function lies at around 1.40 Hz, and the first-mode frequency using the PySimple3 model is 1.38Hz, whereas the first mode frequency using the API sand relation is 1.15 Hz. The API sand model predicts significantly lower first-mode frequency than the test data or the PySimple3 model, which is a clear indication that the subgrade reaction modulus values utilized in the API sand equation are lower than the actual small-strain values. The PySimple3 model is therefore better suited to dynamics problems because it can capture the small-strain nonlinearity and the large-strain behavior using a single set of input parameters.

CONCLUSIONS

The bounding surface plasticity model for the nonlinear p-y behavior of piles in sand during dynamic loading is shown to be superior to the widely used API sand model. Drawbacks with the API sand model are (1) it exhibits the incorrect capacity compared with dynamic test data, (2) uses a strain-compatible secant stiffness rather than a true elastic stiffnes, and (3) the shape of the curve is too linear in the small strain region. The proposed PySimple3 model, implemented in OpenSees, overcomes these limitations and shows better agreement with measurements from a centrifuge test program involving a single pile in sand.

The proposed constitutive model utilizes shear wave velocity to compute the elastic stiffness in the modeling equations, which is a significant improvement over the strain compatible secant modulus in the API sand relation because it better captures the small-strain behavior that can be very important for dynamic problems. A study of ambient vibration data clearly showed that the first-mode frequency is under-predicted using the API sand model, which could have significant consequences for predicting the modal response of a pile-supported structure. Furthermore, V_s is a parameter that is commonly measured as part of a geotechnical site investigation, particularly for earthquake problems where V_{s30} is required for seismic hazard analysis. The PySimple3 formulation therefore provides a rational basis for incorporating more site-specific geotechnical knowledge than the API sand relation.

The formation of a depression around a pile was observed for the strongest shaking events in the centrifuge modeling study. Existing procedures for incorporating gapping between piles and cohesive soils into the p-y response may not capture this mechanism since it occurred in cohesionless soil. More research is needed to better understand this mechanism.

Dynamic p-y capacity observed during many previous studies is larger than the API sand equations predict. Reasons for this may include radiation damping and strain rate effects, but more research is required to fully understand this feature of behavior.

ACKNOWLEDGEMENTS

This work was supported by the National Research Foundation (NRF) grant funded by the Korea government (MEST) (No. 2010-0018864) and the SNU SIR Group of the BK21 research Program funded by the Ministry of Education, Science and Technology.

REFERENCES

American Petroleum Institute (API). (1993). "Recommended practice for planning, designing and constructing fixed offshore platforms." API RP 2A-WSD, 20th ed., American Petroleum Institute, Washington DC.

Bolton, M.D. (1986). "The strength and dilatancy of sands." *Geotechnique*, 36(1), pp.65-78.

Boulanger, R.W., Kutter, B.L., Brandenberg, S.J., Singh, P., and Chang, D. (2003). Pile Foundations in Liquefied and Laterally Spreading Ground during Earthquakes: Centrifuge Experiments and Analyses. Report No. UCD/CGM-03/01, Center for Geotechnical Modeling, Department of Civil Engineering, University of California, Davis, CA, 205 pp.

Brandenberg, S.J., Wilson, D.W., and Rashid, M.M. (2010). "Weighted Residual Numerical Differentiation Algorithm Applied to Experimental Bending Moment Data", *J. Geotech. Geoenviron. Eng.*, 136(6), pp.854-863.

Brandenberg, S.J., Zhao, M., Boulanger, R.W.,, and Wilson, D.W. (2013). "p-y plasticity model for nonlinear dynamic analysis of piles in liquefiable soil." *J. Geotech. Geoenviron. Eng.*, 139(8), pp.1262-1274.

Dafalias, Y.F. (1986). "Bounding surface plasticity. I: Mathematical foundation and hypoplasticity." *J. Eng. Mech.*, 112(9), pp.966-987.

Dafalias, Y.F., and Manzari, M.T. (2004). "Simple plasticity sand model accounting for fabric change effects." *J. Eng. Mech*., 130(6), pp.622–634.

Darendeli, M. (2001). "Development of a new family of normalized modulus reduction and material damping curves." Ph.D Thesis., The University of Texas at Austin, USA, pp.249-272.

Dobry, R., Abdoun, T., O'Rourke. T., and Goh, S.H. (2003). "Single Piles in Lateral Spreads: Field Bending Moment Evaluation." *J. Geotech. Geoenviron. Eng.*, 129(10), pp.879-889.

Gazetas, G. and Dobry, R. (1984). "Horizontal response of piles in layered soils." *J. Geotech. Eng.*, 110(1), pp.20-40.

Hardin, B.O., and Drnevich, V.P. (1972). "Shear modulus and damping in soils: measurement and parameter effects," *J. Soil Mech. Found. Div.*, 98(6), pp.603-624.

Kagawa, T., and Kraft, L.M. (1980). "Seismic p-y response of flexible piles," *J. Geotech. Eng. Div*., 106(GT8), pp.899-918.

Kim, D.S., Kim, N.R., Choo, Y.W., and Cho, G.C. (2013a). "A Newly Developed State-of-the-Art Geotechnical Centrifuge in Korea", *KSCE Journal of Civil Engineering*; 17(1), pp.77-84.

Kim, D.S., Lee, S.H., Choo, Y.W., and Perdriat, J. (2013b). "Self-balanced Earthquake Simulator on Centrifuge and Dynamic Performance Verification", *KSCE Journal of Civil Engineering*; 17(4), pp.651-661.

Lee, S.H., Choo, Y.W., and Kim, D.S. (2013). "Performance of an equivalent shear beam (ESB) model container for dynamic geotechnical centrifuge tests", *Soil Dynamics and Earthquake Engineering*; 44, pp.102-114.

McGann, C., Arduino, P., and Mackenzie-Helnwein, P. (2011). "Applicability of conventional p-y relations to the analysis of piles in laterally spreading soil." *J. Geotech. Geoenviron. Eng.*, 137(6), pp.557-567.

Matlock, H. (1970). "Correlations for design of laterally loaded piles in soft clay," Proc. 2nd Annual Offshore Technology Conference, Paper No. OTC 1204, Houston, Tex., pp.577-594.

Matlock, H., Foo, S.H., and Bryant, L.L. (1978). "Simulation of lateral pile behavior." *Earthquake Engineering and Soil Dynamics*, *Proceedings of the ASCE Geotechnical Engineering Division*, ASCE, Reston, VA., pp. 600-619.

McKenna, F., Scott, M. H., and Fenves, G. L. (2010). "Nonlinear finite element analysis software architecture using object composition." *J. Comput. Civ. Eng.*, 24(1), pp.95–107.

Rollins, K.M., Lane, J.D., and Gerber, T.M. (2005). "Measured and computed lateral response of a pile group in sand." *J. Geotech. Geoenviron. Eng.*, 131(1), pp.103-114.

Simo, J. C., and Hughes, T. J. R. (1998). Computational inelasticity, Springer, New York.

Varun, V. (2010). "A nonlinear dynamic macroelement for soil structure interaction analyses in liquefiable sites." Ph.D. thesis, School of Civil and Environmental Engineering, Georgia Institute of Technology, Atlanta.

Yang, E.K., Choi, J.I., Kown, S.Y., Kim, M.M. (2011). "Development of dynamic p-y backbone curves for a single pile in dense sand by 1g shaking table tests.", *KSCE Journal of Civil Engineering*, 15(5), pp.813-821.

Yamada, S., Hyodo, M., Orense, R. P., Dinesh, S. V., and Hyodo, T. (2008). "Strain-dependent dynamic properties of remolded sand-clay mixtures." *J. Geotech. Geoenviron. Eng.*, 134(7), pp.972–981.

Yoo, M.T., Choi, J.I., Han, J.T., and Kim, M.M. (2013). "Dynamic p-y Curves for Dry Sand by Dynamic Centrifuge Tests", *Journal of Earthquake Engineering*, 17(7), pp.1082-1102.

Figure Captions

Figure 1. Schematic of bounding surface model behavior.

Fig. 2. Dimensionless plot demonstrating model behavior.

Figure 3. Schematic layout and instrumentation for model soil-pile system (model scale).

Figure 4. Experimental dynamic p-y curves: (a) 0.5m depth, (b) 1.5m depth.

Figure 5. Dynamic backbone and monotonic cyclic backbone p-y relations for centrifuge test in sand (Yoo et al. 2012).

Figure 6. Experimental p-y backbone curve and API p-y curves (a) 0.5m depth, (b) 1.5m depth.

Figure 7. Comparison of the acceleration at the superstructure between analysis results using proposed p-y model and centrifuge test results.

Figure 8. Comparison of the peak bending moment between analysis results using proposed p-y model and centrifuge test results.

Figure 9. Analysis results with uppermost p-y element (at a depth of 0.5m) removed due to formation of depression around pile.

Figure 10. Ambient vibration transfer function compared with first mode Eigenvalues from p-y analysis.

Table 1 Properties of a model pile

Pile Property	Prototype	Model
Diameter, *B* (cm)	100	2.5
Wall Thickness, *t* (cm)	1.2	0.1
Material	Steel	Aluminum
Flexural rigidity, *EI* ($N \cdot cm^2$)	9.54E+12	3.76E+6
Mass attached to pile head (kg)	64,000	1.0
Embedment depth (cm)	2,280	57

Table 2 Properties of Jumoonjin sand

D_{10} (mm)	D_{50} (mm)	C_u	G_s	$\gamma_{d,\ max}$ (kN/m^3)	$\gamma_{d,\ min}$ (kN/m^3)
0.37	0.60	1.77	2.64	16.6	13.3

Table 3. Base motion sequence (prototype scale).

Case No.	Peak Base Acceleration (g)	Peak Surface Acceleration (g)	Peak Superstructure Acceleration (g)
1	0.05	0.08	0.18
2	0.1	0.15	0.29
3	0.15	0.28	0.45
4	0.23	0.44	0.65
5	0.3	0.76	0.82
6	0.4	0.87	0.88

Figure 1
Click here to download high resolution image

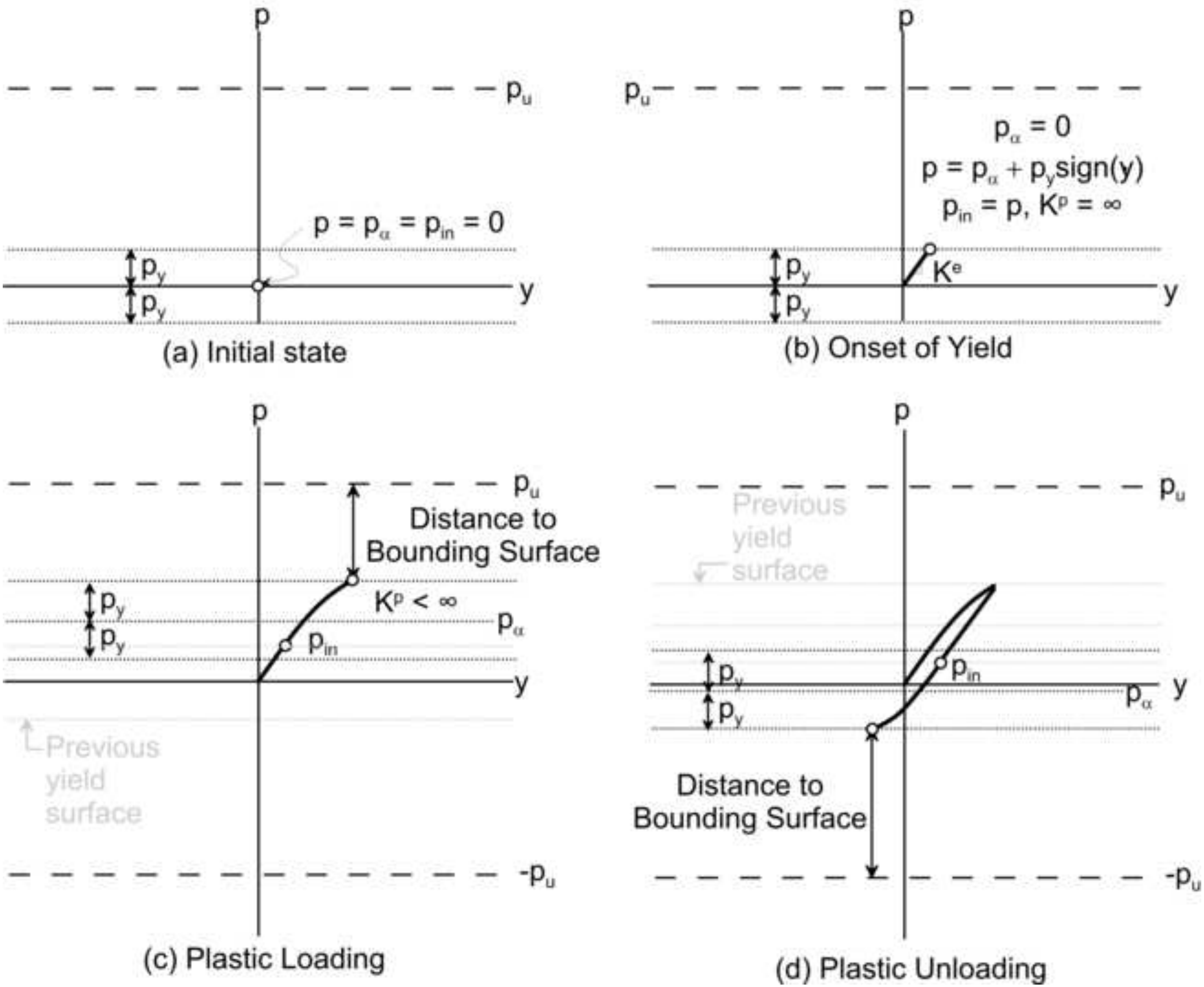

Figure 2
Click here to download high resolution image

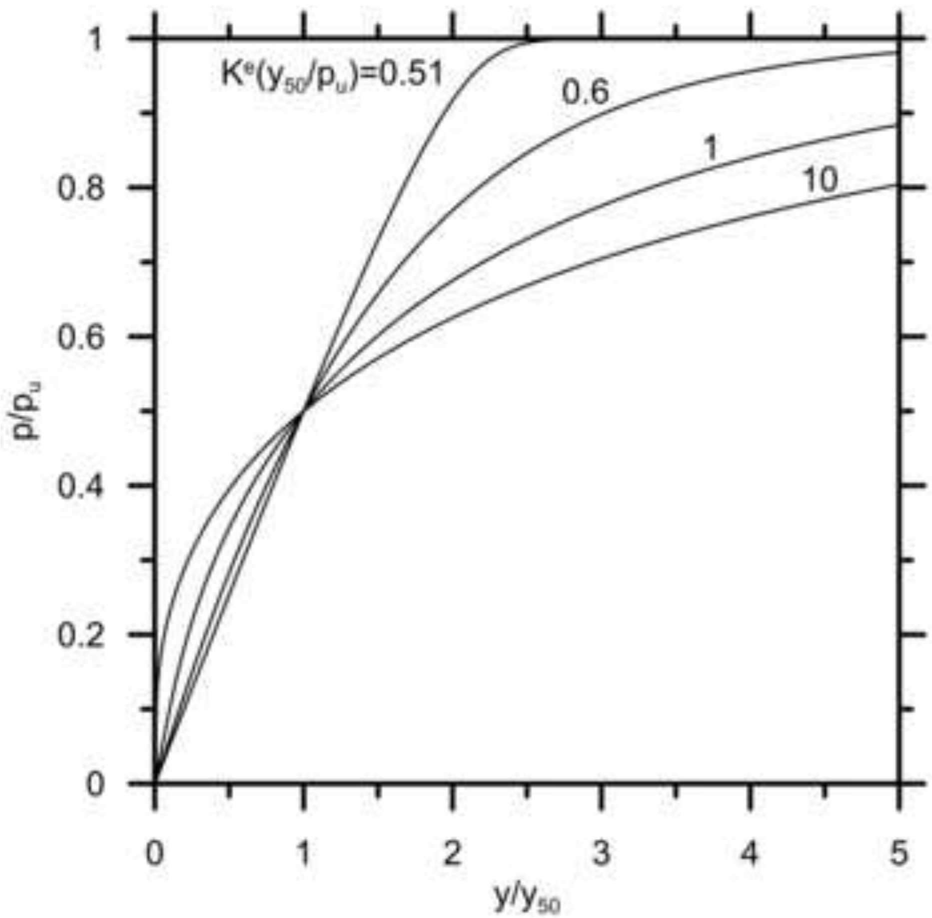

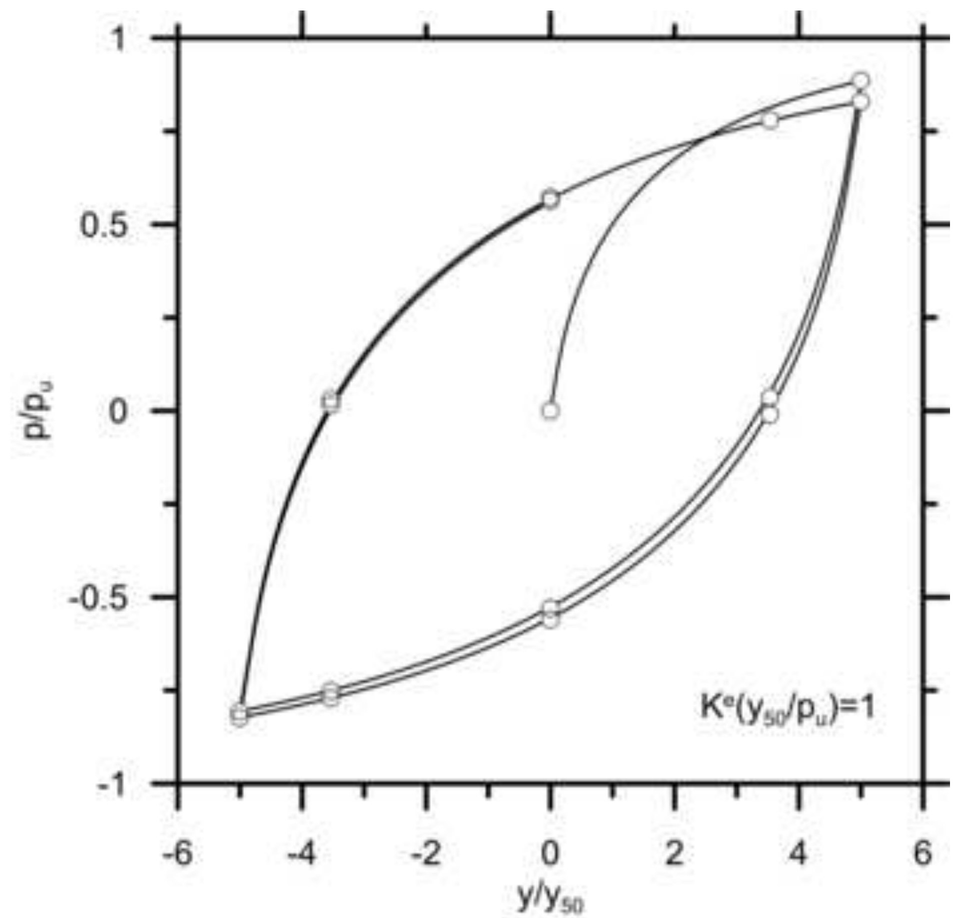

Figure 3
Click here to download high resolution image

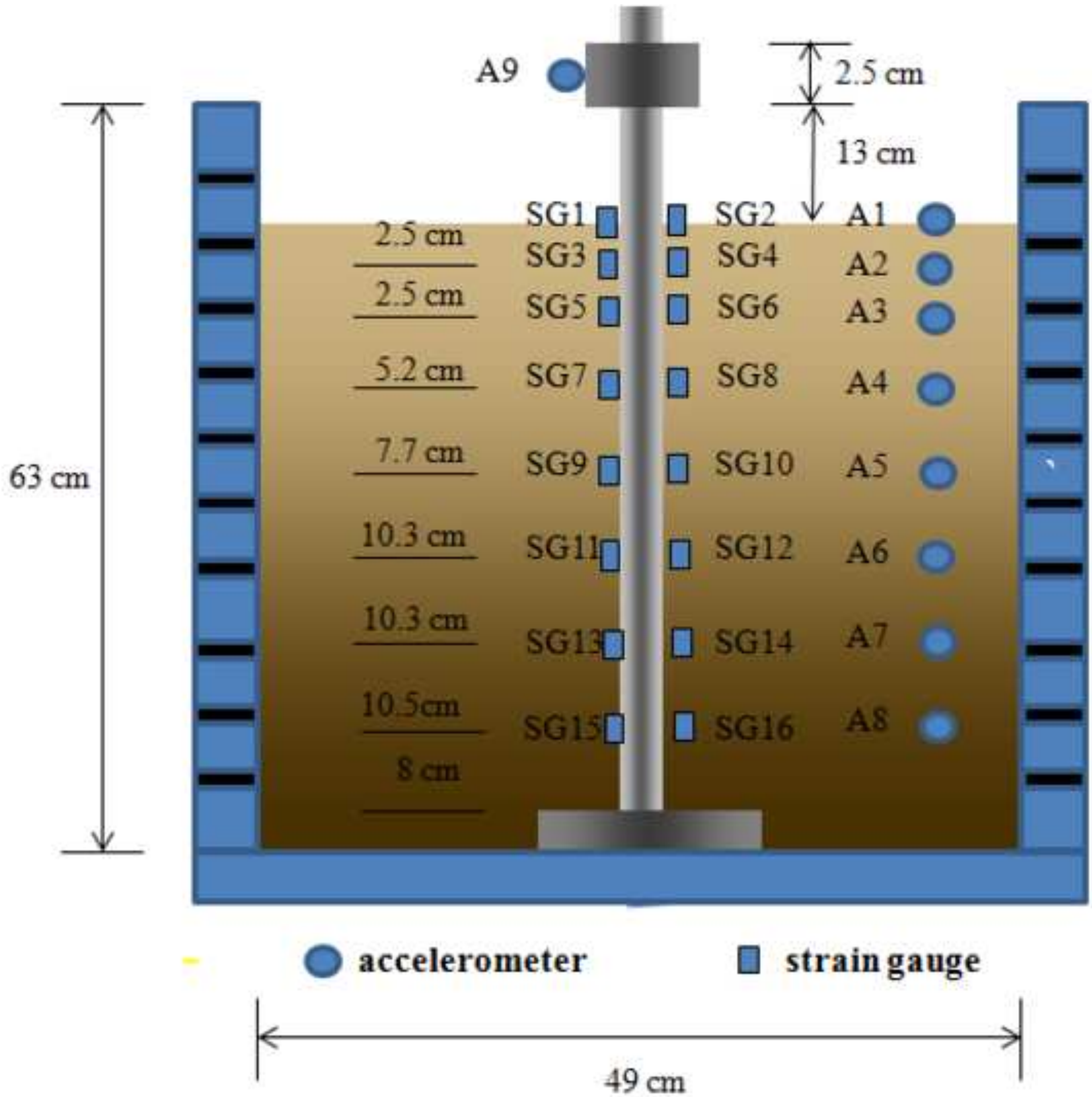

Figure 4
Click here to download high resolution image

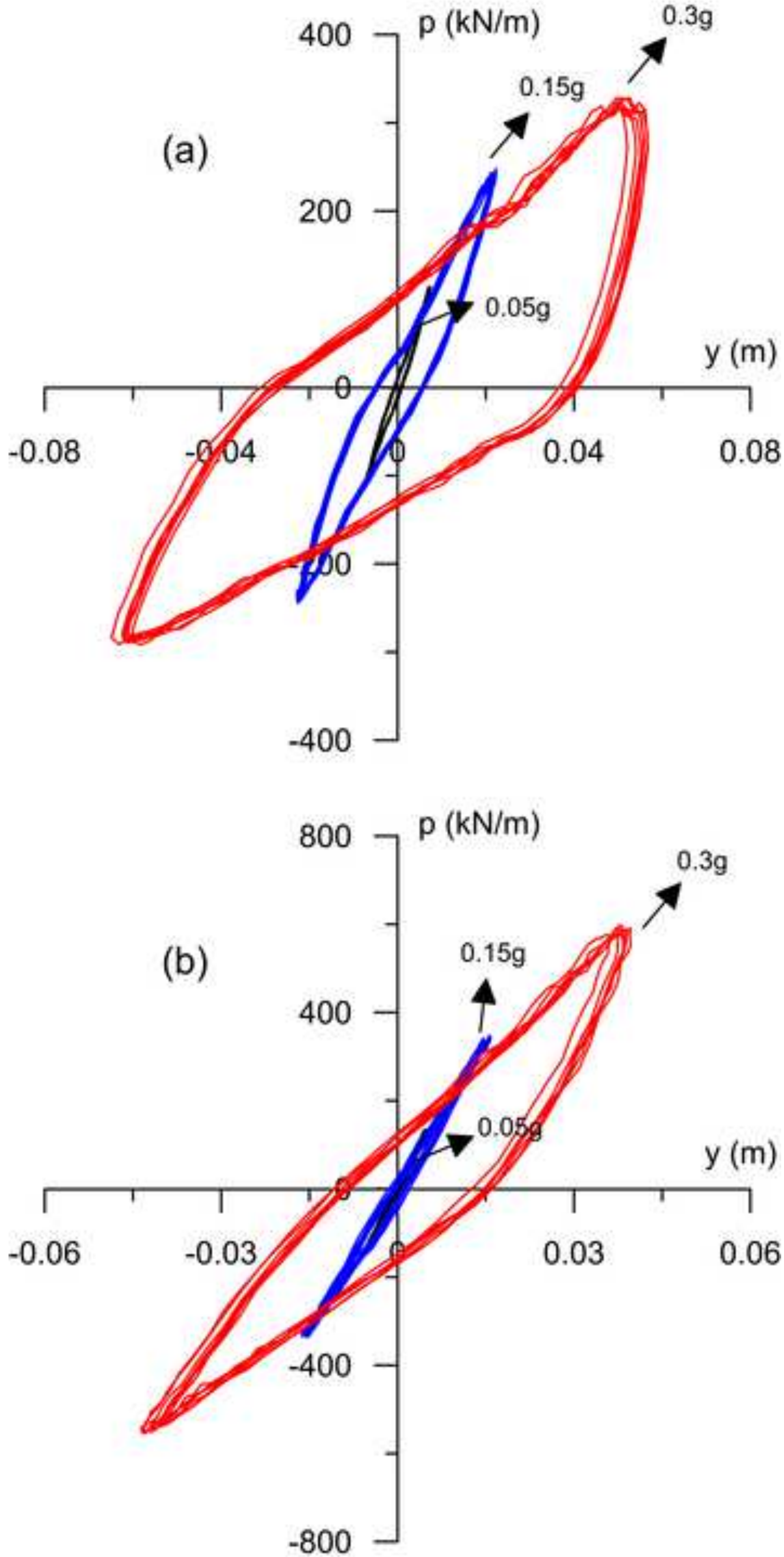

Figure 5
Click here to download high resolution image

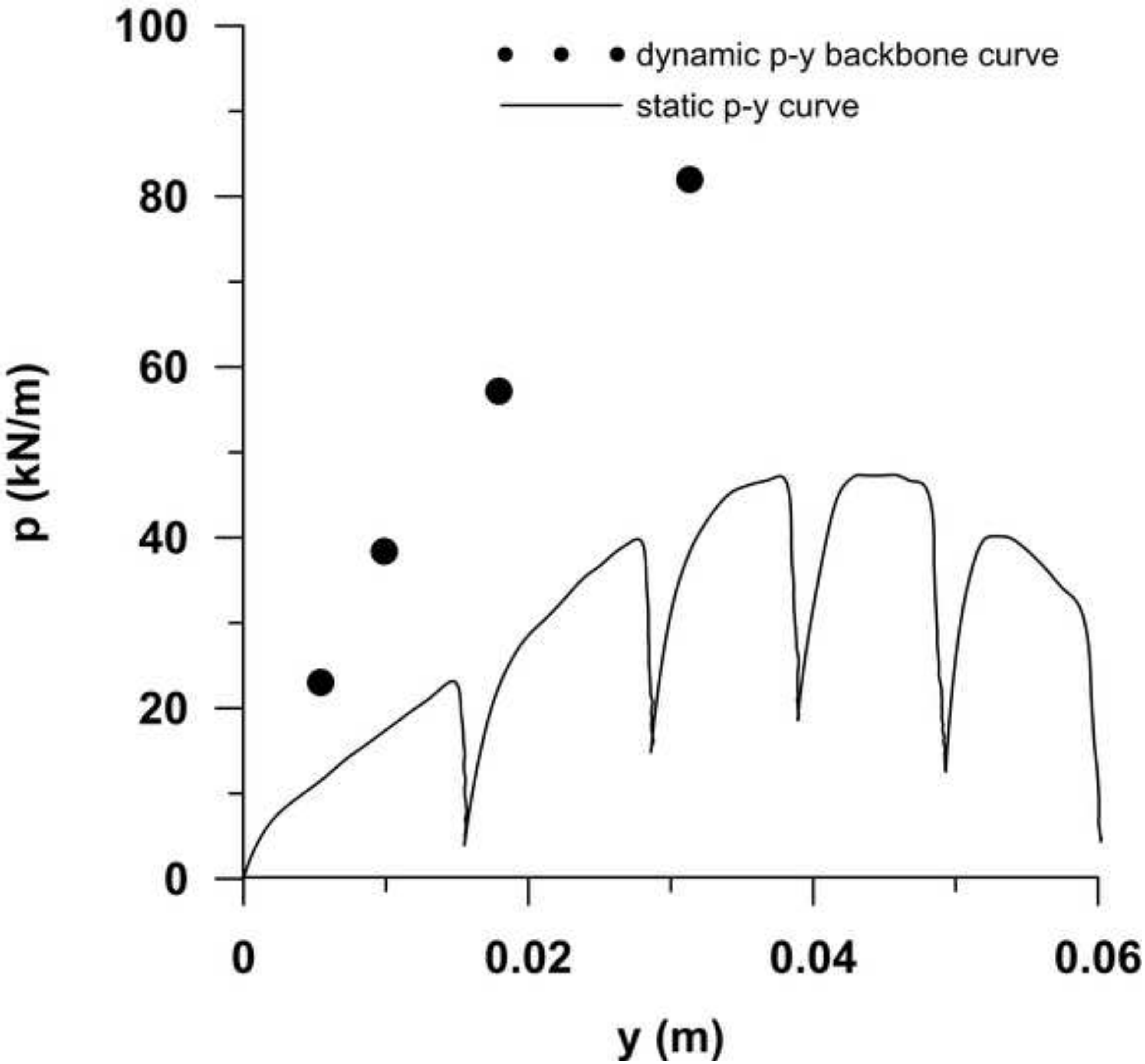

Figure 6
Click here to download high resolution image

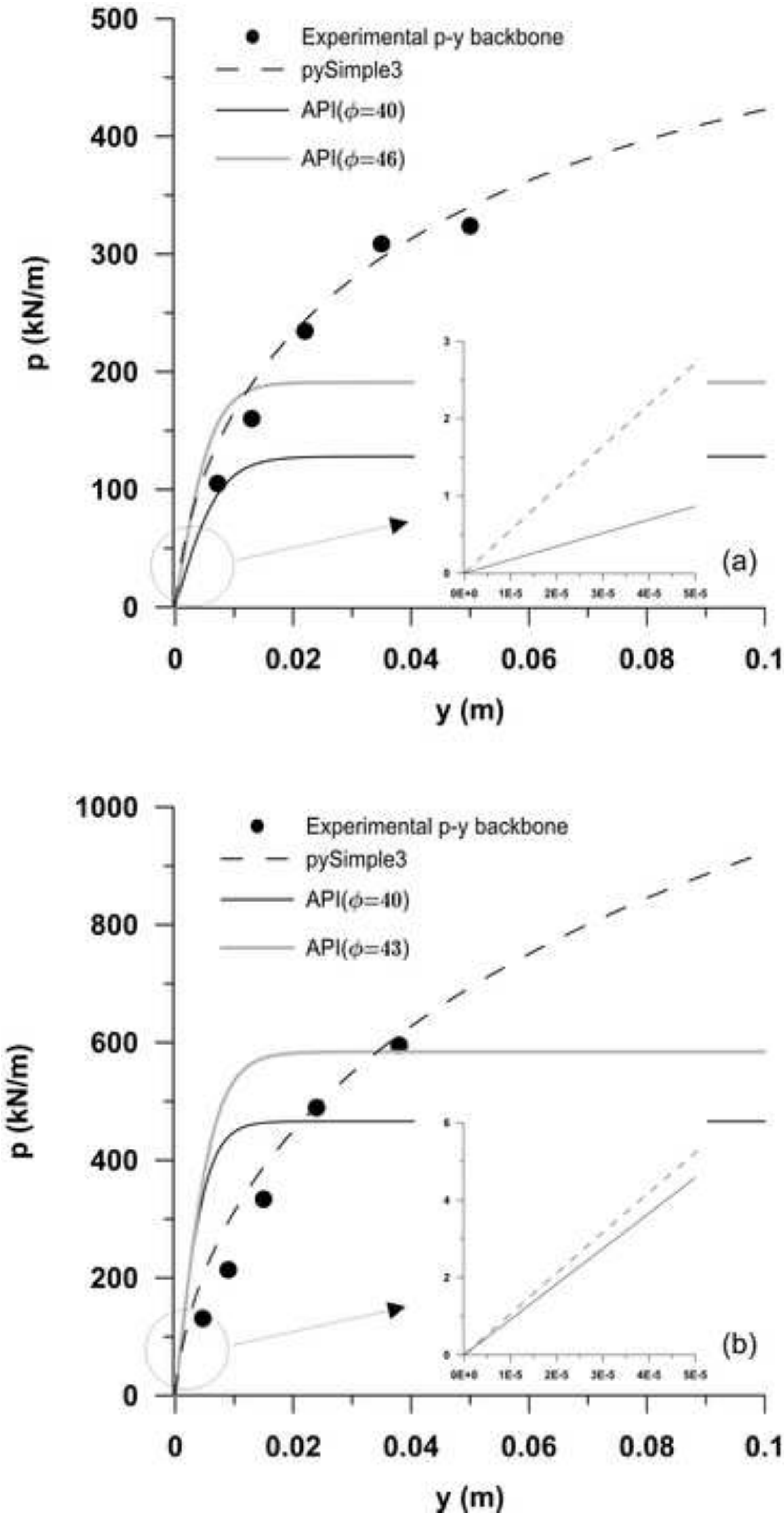

Figure 7
Click here to download high resolution image

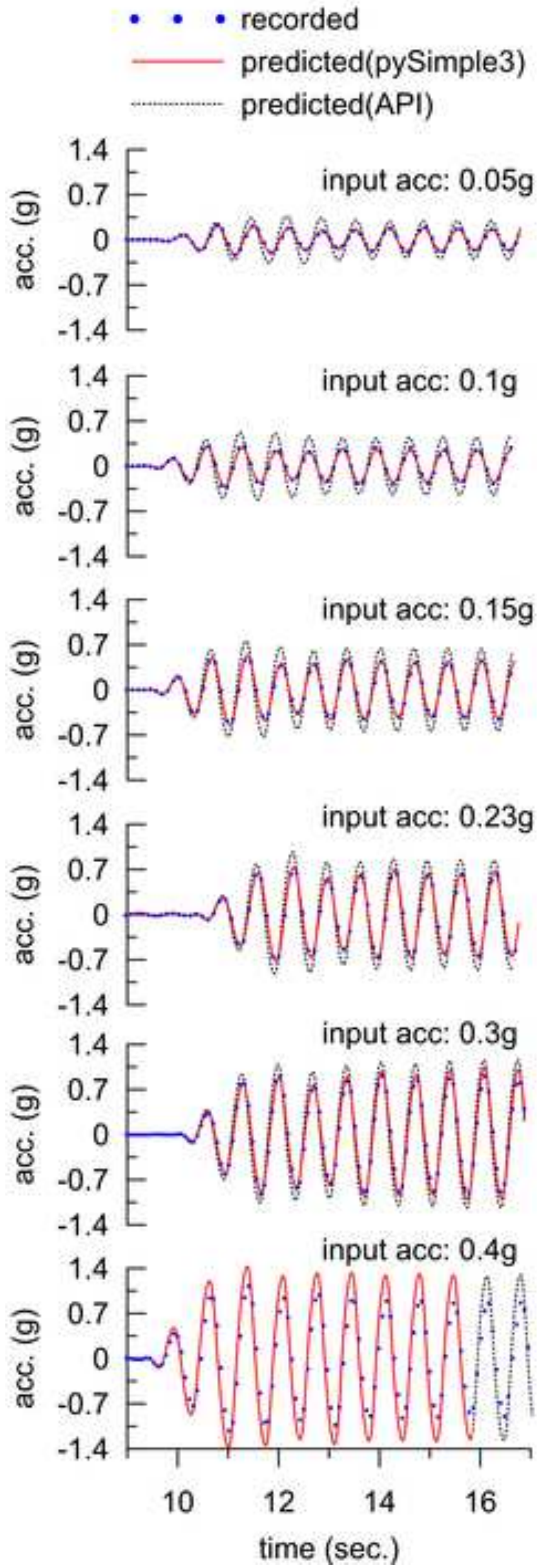

Figure 8
Click here to download high resolution image

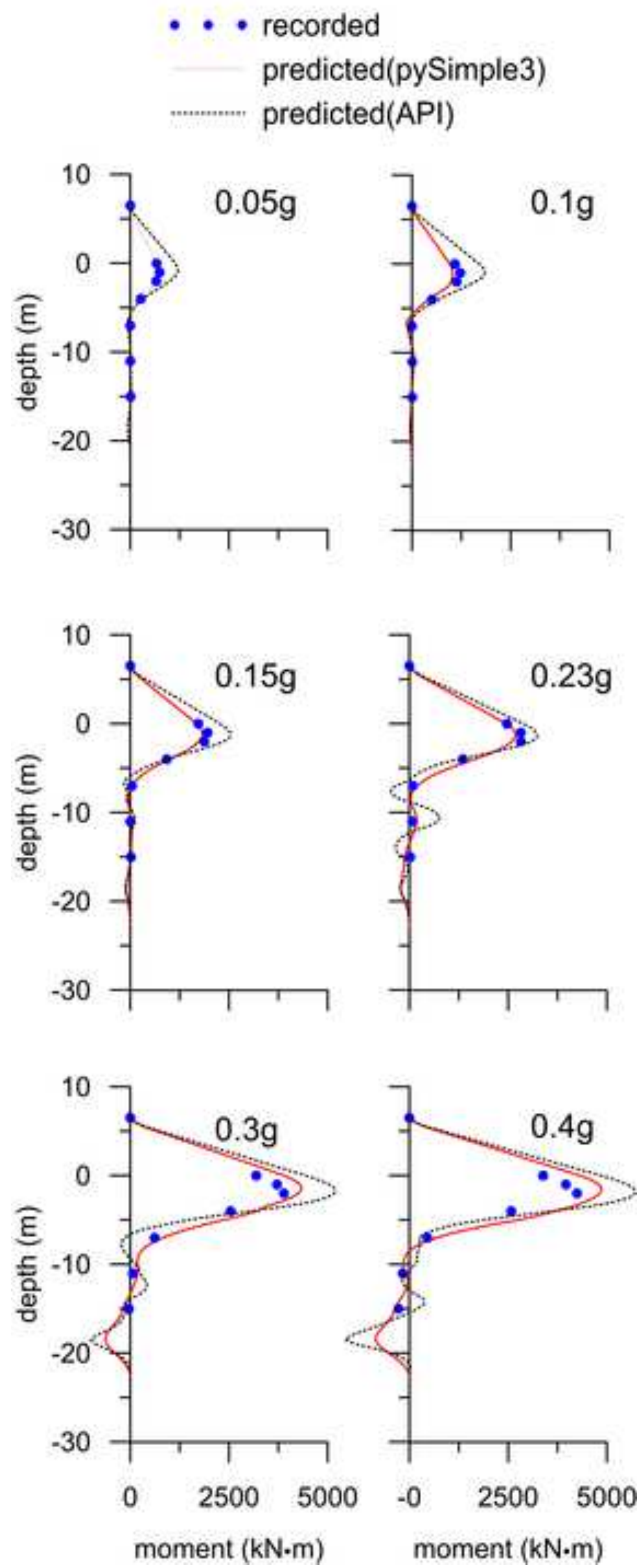

Figure 9
Click here to download high resolution image

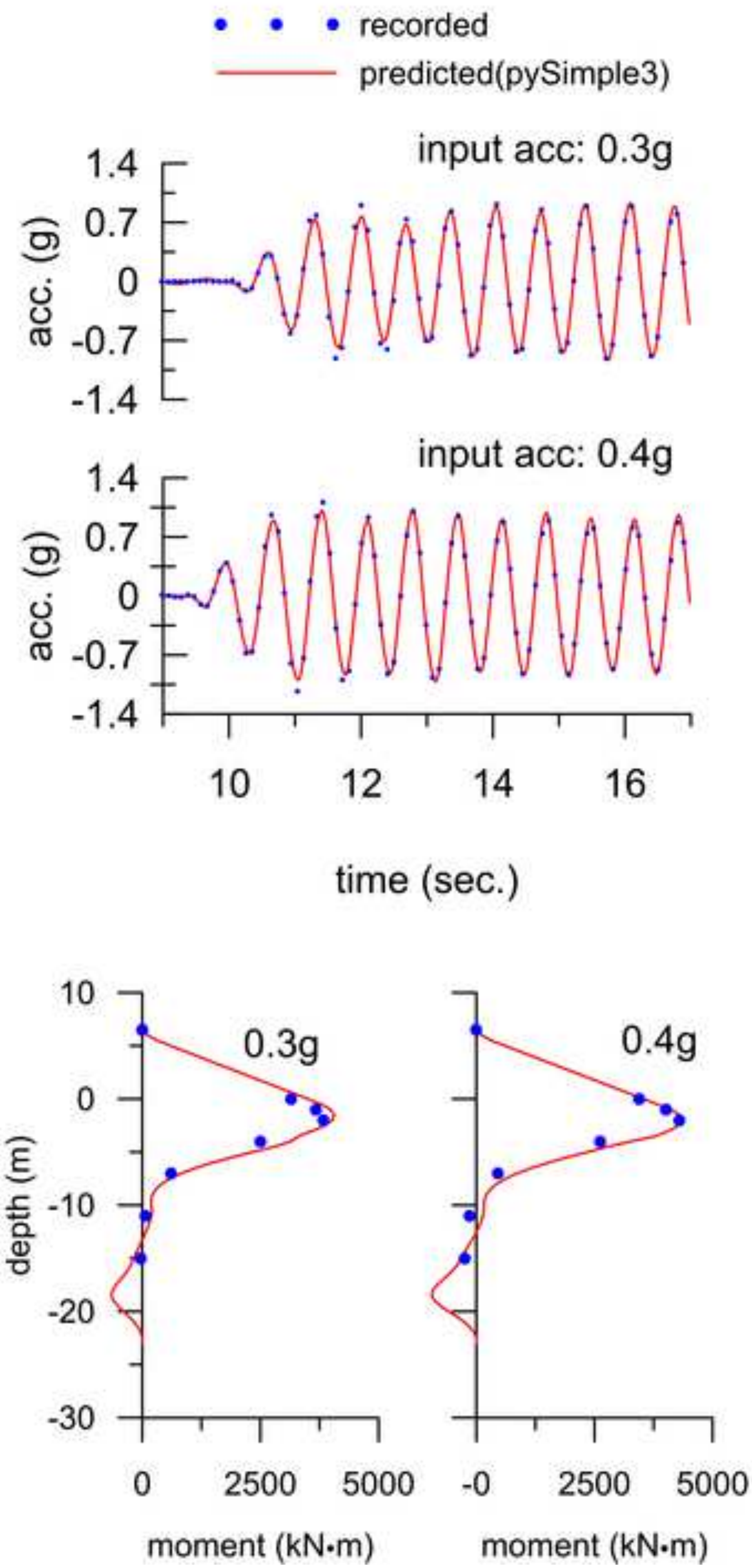

Figure 10
Click here to download high resolution image